Journal of Applied Physics ARTICLE pubs.aip.org/aip/jap

Optimizing hybrid ferromagnetic metal–ferrimagnetic insulator spin-Hall nano-oscillators: A micromagnetic study

Cite as: J. Appl. Phys. **136**, 193901 (2024); doi: 10.1063/5.0232164
Submitted: 5 August 2024 · Accepted: 28 October 2024 ·
Published Online: 15 November 2024

View Online Export Citation CrossMark

Robert Xi, Ya-An Lai,[a] and Andrew D. Kent[b]

AFFILIATIONS

Center for Quantum Phenomena, Department of Physics, New York University, New York, New York 10003, USA

[a]**Author to whom correspondence should be addressed:** yal245@nyu.edu
[b]andy.kent@nyu.edu

ABSTRACT

Spin-Hall nano-oscillators (SHNOs) are nanoscale spintronic devices that generate high-frequency (GHz) microwave signals useful for various applications, such as neuromorphic computing and creating Ising systems. Recent research demonstrated that hybrid SHNOs consisting of a ferromagnetic metal (permalloy) and lithium ferrite-based (LAFO) insulating ferrimagnetic thin films have advantages in having lower auto-oscillation threshold currents (I_{th}) and generating larger microwave output power, making this hybrid structure an attractive candidate for spintronic applications. It is essential to understand how the tunable material properties of LAFO, e.g., its thickness, perpendicular magnetic anisotropy ($K_{u,LAFO}$), and saturation magnetization ($M_{s,LAFO}$), affect magnetic dynamics in hybrid SHNOs. We investigate the change in I_{th} and the output power of the device as the LAFO parameters vary. We find the I_{th} does not depend strongly on these parameters, but the output power has a highly nonlinear dependence on $M_{s,LAFO}$ and $K_{u,LAFO}$. We further investigate the nature of the excited spin-wave modes as a function of $K_{u,LAFO}$ and determine a critical value of $K_{u,LAFO}$ above which propagating spin-waves are excited. Our simulation results provide a roadmap for designing hybrid SHNOs to achieve targeted spin excitation characteristics.

I. INTRODUCTION

Spin-Hall nano-oscillators (SHNOs) have been of great research interest in achieving highly efficient spintronic devices for applications in the field of magnonics[1–3] and other novel information processing architectures, such as Ising systems,[4–6] data communication,[7,8] and neuromorphic computing.[9–14] SHNO typically consists of a heavy metal (HM) layer and a ferromagnetic layer (FM) in which spin–orbit torque is generated by the spin-Hall effect in the HM layer that drives magnetic moments to auto-oscillation in the FM layer.[15–18] Insulating ferrimagnetic layers have been shown to effectively transmit spin angular momentum due to their low magnetic damping, associated with their lack of conduction electrons.[19]

Recent studies have developed a new class of magnetic insulating thin films, lithium aluminum ferrite (LAFO), which possesses desirable properties for SHNO integration, such as tunable magnetic anisotropy, magnetization, low damping, and absence of dead magnetic layers.[20] A recent study demonstrated that a hybrid SHNO configuration consisting of a permalloy/platinum bilayer nanowire (Py/Pt) on top of an extended LAFO thin film enhances microwave power emission and leads to excitation of localized spin-wave edge modes.[21] With the tunability of LAFO properties, it is essential to understand how the thickness, saturation magnetization ($M_{s,LAFO}$), and magnetic anisotropy ($K_{u,LAFO}$) of LAFO affect the auto-oscillation threshold currents and the amplitude of the modes. More importantly, as propagating spin-waves can be excited in SHNO consisting of materials with perpendicular magnetic anisotropy (PMA),[22,23] it is also essential to investigate the role of PMA in hybrid SHNO.

In this study, we use micromagnetic methods to study the effect of LAFO thickness, $M_{s,LAFO}$, and $K_{u,LAFO}$ on SHNO characteristics. We find the critical current for the onset of auto-oscillations to be relatively insensitive to magnetization and perpendicular magnetic anisotropy. However, as the perpendicular magnetic anisotropy increases, the nature of the excited spin-waves changes from localized bulk and edge modes to propagating spin-wave modes and then to localized droplet

modes. Our simulation findings, thus, provide insights into the design of hybrid SHNOs to obtain desired spin excitation characteristics.

II. MICROMAGNETIC SIMULATIONS

We used the MuMax3 micromagnetic solver[24] to simulate a LAFO/Py/Pt hybrid SHNO device. We model a $400 \times 1500 \times 5\,\mathrm{nm}^3$ Py nanowire on top of a $1500 \times 1500 \times t\,\mathrm{nm}^3$ ($t = 0-40$ nm) LAFO layer, as shown in Fig. 1(a). The simulation employs a cell size of $5 \times 5 \times 5\,\mathrm{nm}^3$, which is about the exchange length of Py (5.3 nm) and well below that of LAFO (12–31 nm for the range of LAFO parameters we consider, see below). Py parameters are kept constant throughout simulations: $\mu_0 M_{s,\,\mathrm{Py}} = 1.08$ T, an effective magnetization $\mu_0 M_{\mathrm{eff},\,\mathrm{Py}} = 0.78$ T, which is defined as $M_{\mathrm{eff}} = M_s - 2K_u/\mu_0 M_s$, and a Gilbert damping constant $\alpha_{\mathrm{Py}} = 2.6 \times 10^{-2}$ from ferromagnetic resonance (FMR) measurements.[21] The following LAFO properties are fixed throughout our study: the exchange stiffness is 4 pJ/m and the Gilbert damping $\alpha_{\mathrm{LAFO}} = 1 \times 10^{-3}$. The exchange constant between the Py layer and LAFO layer is taken to be half of the harmonic mean of the two layers. Near the boundaries of the simulated region, we set an exponentially increased damping to reduce spin-wave reflection. To properly model the demagnetization field in the extended LAFO, periodic boundary conditions are applied in the $\hat{x}$ direction, the direction transverse to the electrical current application.

To simulate auto-oscillation excitation, we apply an external magnetic field at 70° with respect to the $\hat{y}$ direction, the central axis of the Py nanowire. In the experiment, the auto-oscillation signal is detected by the anisotropic magnetoresistance effect. Therefore, the magnetic field must be applied at some angle to the direction of the electrical current. An electrical current is applied to a Py/Pt bilayer to excite auto-oscillation. Thus, spins in the Pt nanowire at the interface to Py are polarized in the $\hat{x}$ direction. To describe this in micromagnetic simulations, a spin current J_s in the $\hat{x}$ direction is applied to the active region ($500 \times 400 \times 5\,\mathrm{nm}^3$) of the Py nanowire. We neglect the Oersted field generated from J_e since it is less than 10% of the external field from a COMSOL modeling of the magnetic field distribution. The spin current density J_s is calculated from the current density J_e in Pt using the relation $J_s = \theta_{\mathrm{SH}} J_e$, where θ_{SH} is the spin-Hall angle of Pt and is set to 0.15. In the simulations, J_e is slowly increased at a rate of $4 \times 10^8\,\mathrm{A/m^2 s}$ so that the system reaches a steady state at each time step of 1 ps. We first determine the threshold current density J_{th} to excite the auto-oscillation state by monitoring whether the average maximum torque acting on the Py magnetization increases within 150 ns. An increased torque implies that the Py magnetization is driven out of equilibrium and into auto-oscillation. To eliminate J_{th}-dependent effects and ensure the system reaches steady-state dynamics in our studies, we apply $J_e = 1.2 J_{\mathrm{th}}$. To resolve the resonant frequencies of the auto-oscillation state, we performed the fast Fourier transform (FFT) on the time evolution of the spatially averaged steady-state magnetization along the z direction $\bar{m}_z(t)$ in the central Py nanowire. The initial 40 ns of the simulation were excluded in the FFT analysis to ensure the transient dynamics is not included. We find the auto-oscillation frequencies and corresponding amplitude by fitting the resulting FFT amplitude spectrum to a Lorentzian function. In an experiment, the magnetization precession leads to resistance oscillations through the anisotropic magnetoresistance effect that generate the microwave signal.[25,26] Larger amplitude precession, thus, leads to higher output power. Since the FFT in the simulation is proportional to the amplitude of the magnetization precession, we can use this property to infer the output power. Pixel-wise spatial FFT is conducted to obtain the spatial profile for each oscillation mode in the Py nanowire and LAFO layer following the FFT method of Ref. 27. To simulate FMR experiments, an in-plane perturbing magnetic field in the form of a sinc function of a magnitude 0.5 mT is applied uniformly to the sample, which is subjected to $H_{\mathrm{ext}} = 0.08$ T. Then, we perform FFT on the excited $\bar{m}_z(t)$ to determine the FMR frequencies.

III. RESULTS AND DISCUSSION

Previous work has shown that the main auto-oscillation modes in LAFO/Py/Pt hybrid SHNO devices are an edge mode (EM) and a bulk mode (BM).[21] For EMs, the auto-oscillation occurs at a lower frequency with a higher oscillation amplitude near the edges of the Py nanowire, where the internal magnetic field is reduced due to the

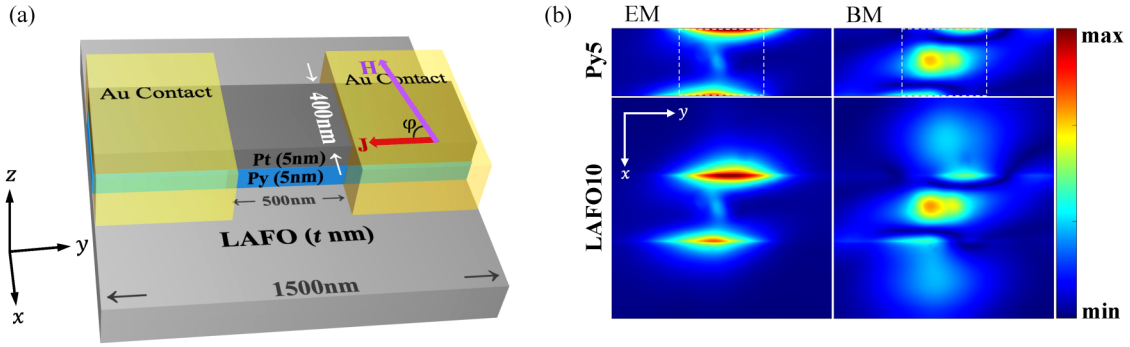

FIG. 1. Hybrid nano-oscillator and modes spatial FFT images. (a) Schematic of a hybrid SHNO. The device consists of LAFO (t_{LAFO})/Py5/Pt5. The external field is applied at an angle ϕ to the current, and the applied charge current is restricted to the center region of the Py nanowire, indicated in a dark blue color. (b) Spatial FFT profiles of the edge mode (EM) and bulk mode (BM) in the Py nanowire and LAFO (10 nm) layer. An in-plane external field $\mu_0 H_{\mathrm{ext}} = 0.08$ T is applied at $\phi = 70°$. The region enclosed by the white broken lines denotes the area where the spin current is injected into the Py layer.

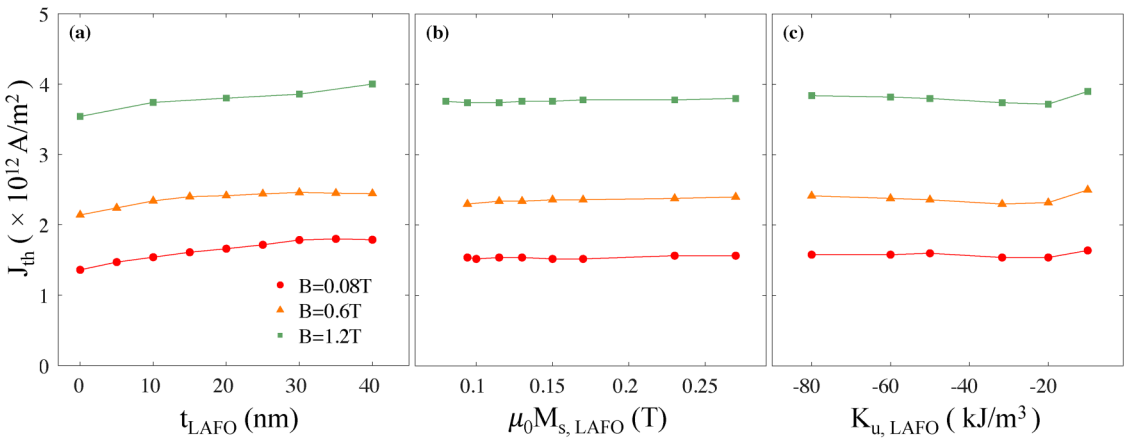

FIG. 2. Threshold current density J_{th} as a function of (a) LAFO thickness t_{LAFO} ($\mu_0 M_{s,\,LAFO} = 0.0942$ T, $K_{u,LAFO} = -31.7$ kJ/m^3), (b) LAFO saturation magnetization $M_{s,LAFO}$ ($t_{LAFO} = 10$ nm, $K_{u,LAFO} = -31.7$ kJ/m^3), and (c) LAFO perpendicular anisotropy constant $K_{u,LAFO}$ ($t_{LAFO} = 10$ nm, $\mu_0 M_{s,LAFO} = 0.0942$ T) with an in-plane external field $\mu_0 H_{ext} = 0.08$, 0.6, and 1.2 T at $\phi = 70°$. For all the simulations, $\alpha_{LAFO} = 1 \times 10^{-3}$, $\alpha_{Py} = 2.6 \times 10^{-2}$, $\mu_0 M_{eff,Py} = 0.78$ T, and $\mu_0 M_{s,Py} = 1.08$ T.

demagnetizing field. For the BM, the auto-oscillation occurs at high frequency with a high oscillation amplitude near the center of the Py nanowire, as shown in Fig. 1(b).

A. Threshold current

Lowering the threshold current to drive auto-oscillation is crucial to minimize power consumption and heat generation, which affect the thermal stability of SHNO devices. Therefore, we first examine the effect on J_{th} as LAFO thickness (t_{LAFO}), magnetization ($M_{s,LAFO}$), and perpendicular magnetic anisotropy ($K_{u,LAFO}$) at $\mu_0 H_{ext} = 0.08$, 0.6, and 1.2 T. A macrospin model[21] predicts that J_{th} is proportional to t_{LAFO}, $M_{s,LAFO}$, and $K_{u,LAFO}$,

$$J_{th} \propto \left(\alpha_{Py} M_{s,\,Py} t_{Py} + \alpha_{LAFO} M_{s,LAFO} t_{LAFO}\right) \bar{M}_{eff}, \tag{1}$$

where

$$\bar{M}_{eff} = \frac{t_{Py} M_{eff,Py} M_{s,Py} + t_{LAFO} M_{eff,LAFO} M_{s,LAFO}}{t_{Py} M_{s,Py} + t_{LAFO} M_{s,LAFO}} \tag{2}$$

is the average effective magnetization of the hybrid nano-oscillator, and the effective magnetization for Py and LAFO layers is denoted

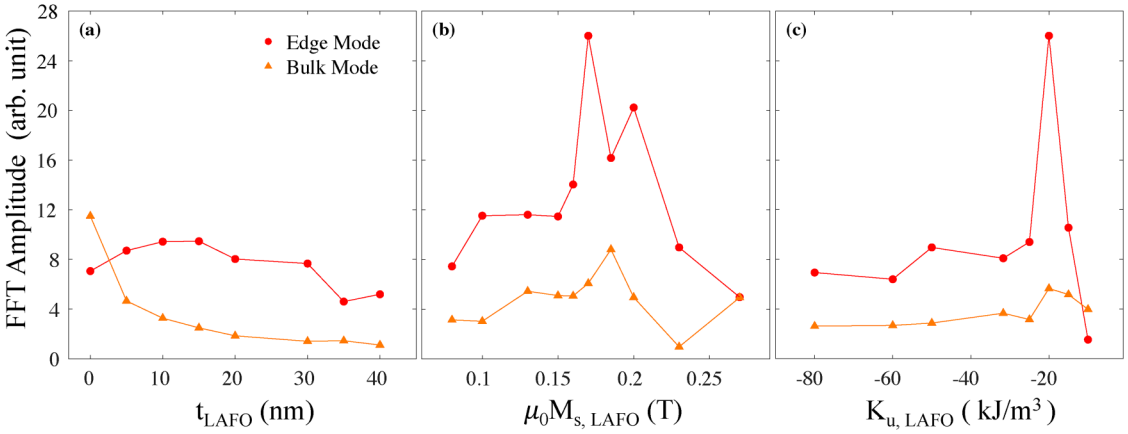

FIG. 3. Edge mode and bulk mode output power as a function of (a) LAFO thickness t_{LAFO} ($\mu_0 M_{s,Py} = 1.08$ T, $K_{u,LAFO} = -31.7$ kJ/m^3). (b) LAFO saturation magnetization $\mu_0 M_{s,LAFO}$ ($t_{LAFO} = 10$ nm, $K_{u,LAFO} = -31.7$ kJ/m^3). (c) LAFO perpendicular anisotropy constant $K_{u,LAFO}$ ($t_{LAFO} = 10$ nm, $\mu_0 M_{s,LAFO} = 0.0942$ T). All simulations were conducted with an in-plane $\mu_0 H_{ext} = 0.08$ T at $\phi = 70°$ with constant parameters $\alpha_{LAFO} = 1 \times 10^{-3}$, $\alpha_{Py} = 2.6 \times 10^{-2}$, $\mu_0 M_{eff,\,Py} = 0.78$ T, and $\mu_0 M_{s,Py} = 1.08$ T. The current density is set to $J_e = 1.2 J_{th}$.

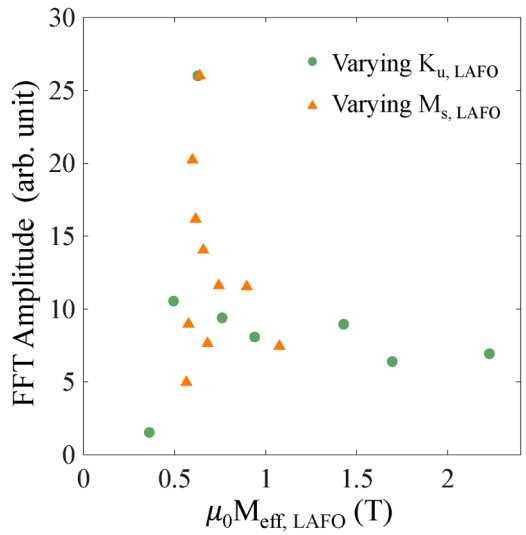

FIG. 4. Edge mode output power as a function of LAFO effective magnetization $M_{\text{eff,LAFO}}$. The effective magnetization is calculated for two cases. First, fix $\mu_0 M_{s,\text{LAFO}} = 0.0942$ T and vary $K_{u,\text{LAFO}}$ (red circles). Second, fix $K_{u,\text{LAFO}} = -31.7\,\text{kJ/m}^3$ and vary $M_{s,\text{LAFO}}$ (orange triangles). The external field is fixed at $\mu_0 H_{\text{ext}} = 0.08$ T at $\phi = 70°$.

by $M_{\text{eff,Py}}$ and $M_{\text{eff,LAFO}}$, respectively. Figure 2(a) shows that J_{th} slowly increases with t_{LAFO}, which agrees with the macrospin model prediction. However, J_{th} does not depend noticeably on $M_{s,\text{LAFO}}$ and $K_{u,\text{LAFO}}$, as seen in Figs. 2(b) and 2(c). We attribute this to the fact that $M_{s,\text{LAFO}}$ is only one-tenth that of $M_{s,\text{Py}}$, leading to a negligible effect on J_{th}, as expected from Eq. (1). From our micromagnetic study, we conclude that in the regime of $0.08\,\text{T} < \mu_0 M_{s,\text{LAFO}} < 0.25\,\text{T}$ and $0.35\,\text{T} < \mu_0 M_{\text{eff,LAFO}} < 2.59\,\text{T}$, reducing t_{LAFO} is the most effective means to lower J_{th}.

B. Output power

It is also crucial to maximize the output power, as it allows better detection of electrical signals in applications. Research has demonstrated that the incorporation of an extended LAFO thin film beneath a Pt/Py nanowire can significantly enhance power emission.[21] However, the relationship between this enhanced power emission and LAFO parameters is yet to be explored. Now, we consider how the output power varies with the LAFO parameters (t_{LAFO}, $M_{s,\text{LAFO}}$, and $K_{u,\text{LAFO}}$). The auto-oscillation amplitude is shown as a function of these parameters in Fig. 3. Figure 3(a) shows that the output power of the EM does not depend strongly on t_{LAFO}, whereas the output power of the BM decreases as t_{LAFO} increases.

Interestingly, Fig. 3(b) shows that there is a peak in the output power of EM and BM around $\mu_0 M_{s,\text{LAFO}} = 0.17$ T. In Fig. 3(c), a peak in EM output power is observed around $K_{u,\text{LAFO}} = -20\,\text{kJ/m}^3$. $M_{\text{eff,LAFO}}$ decreases as $K_{u,\text{LAFO}}$ increases (i.e., in-plane magnetization is less favored). This is advantageous for aligning the moments at the edge of the Py nanowire, generating a larger precession angle. To better understand why there is a maximum in the output power of the EM, $\mu_0 M_{\text{eff,LAFO}}$ is plotted against the EM output power in Fig. 4 based on data from Figs. 3(b) and 3(c). We observe a peak in the EM output power around $\mu_0 M_{\text{eff,LAFO}} = 0.6$ T when varying either $K_{u,\text{LAFO}}$ or $M_{s,\text{LAFO}}$. This suggests that the peak is determined by the effective magnetization $M_{\text{eff,LAFO}}$, rather than by $K_{u,\text{LAFO}}$ or $M_{s,\text{LAFO}}$ independently.

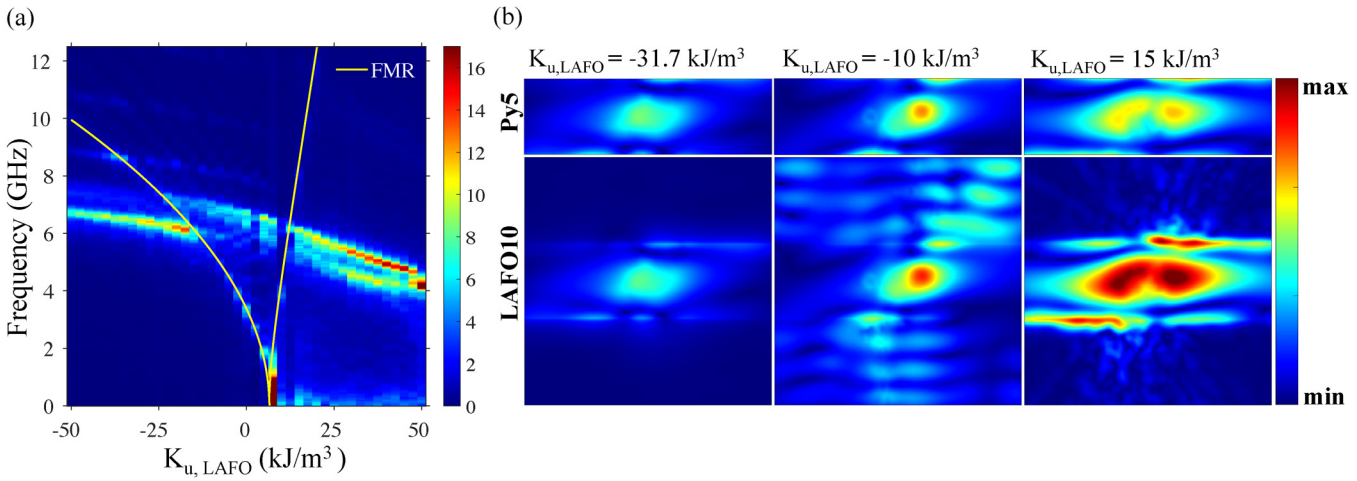

FIG. 5. PSD and spatial profiles from micromagnetic modeling. (a) PSD map as a function of frequency and $K_{u,\text{LAFO}}$ with $\mu_0 H_{\text{ext}} = 0.08$ T at $\phi = 70°$, and $J = 2 \times 10^{12}\,\text{A/m}^2$, $\mu_0 M_{s,\,\text{LAFO}} = 0.0942$ T for LAFO10/Py5. The yellow curve indicates the FMR frequency. (b) Spatial FFT images of the LAFO layer and Py layer at the BM auto-oscillation frequency for $K_{u,\text{LAFO}} = -31.7$, -10, and $15\,\text{kJ/m}^3$. The linear color scale is on the right, where the color represents the FFT amplitude of the magnetization along the z direction.

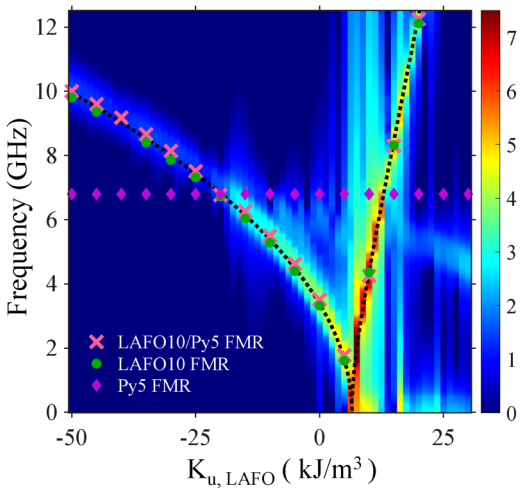

FIG. 6. FMR simulation. PSD of LAFO10/Py5/Pt5 as a function of $K_{u,LAFO}$ at a fixed field $\mu_0 H_{ext} = 0.08$ T at $\phi = 70°$ and fixed saturation magnetization $\mu_0 M_{s,LAFO} = 0.0942$ T and $\mu_0 M_{s,Py} = 1.08$ T. The Kittel model is shown by the black dotted curve. The FMR frequencies of LAFO10/Py5/Pt5, bare LAFO10, and bare Py5 are shown by pink crosses, green circles, and purple diamonds, respectively.

C. Excited mode profiles

We now investigate the nature of the auto-oscillation modes as $K_{u,LAFO}$ is varied. Figure 5(a) shows the power spectral density (PSD) map as a function of frequency and $K_{u,LAFO}$. The yellow curve is the LAFO FMR frequency calculated using the Kittel relation $f = \mu_0\gamma/(2\pi)[(H_{ext}\sin\theta_M - M_{eff}\cos 2\theta_M)(H_{ext}\sin\theta_M - M_{eff}\cos^2\theta_M)]^{1/2}$, where γ is the gyromagnetic ratio, μ_0 is the vacuum permeability and θ_M is the equilibrium angle of the LAFO magnetization and is calculated by solving the angle that minimizes the energy. The PSD map is sectioned into three regions by the FMR curve, where the middle region has spin-wave modes excited at frequencies higher than the FMR frequency f_{FMR} and the other regions have spin-wave modes excited below f_{FMR}. This indicates that the spin-wave modes are localized for both large negative and positive $K_{u,LAFO}$ but can propagate for intermediate values of the perpendicular magnetic anisotropy.[28] This is seen directly by the spatial FFT analysis shown in Fig. 5(b). For large negative $K_{u,LAFO}$, the spin-waves are localized near the Py edges, where the demagnetization field creates a potential well for the spin-waves, associated with a local minima in M_{eff}. The applied field in the plane and the in-plane anisotropy increase the depth of the spin-wave potential well and lead to further mode localization.[29] As $K_{u,LAFO}$ approaches zero from negative values, magnetization has less preference to align along a specific orientation. This leads to a shallower potential well for spin-waves with a smaller M_{eff}. As M_{eff} decreases, the auto-oscillation frequency and f_{FMR} decrease until the auto-oscillation frequency is greater than f_{FMR}, leading to propagating spin-wave modes. For large positive $K_{u,LAFO}$, the LAFO is perpendicularly magnetized. Therefore, increasing $K_{u,LAFO}$ leads to a decreasing M_{eff} but an increasing f_{FMR}.

To better understand the interplay between mode behavior and intrinsic properties of the device, a FMR spectroscopy simulation is conducted with varying $K_{u,LAFO}$, with values ranging from -50 to $30\,kJ/m^3$. Figure 6 compares the PSD FMR map of an LAFO10/Py5/Py5 SHNO device (pink crosses) with the FMR condition derived from the Kittel relation (black dotted curve), the FMR spectrum of LAFO10 (green circles) and Py5 (purple diamonds). The single FMR mode indicates that the LAFO and Py layers are strongly coupled. The similarity in f_{FMR} between the LAFO layer and the device suggests a minimal impact of the Py layer on the hybrid SHNO FMR frequency. In comparison to the data presented in Fig. 5(a), it is observed that the EM's peak output power corresponds to the point where $f_{FMR,Py}$ and $f_{FMR,LAFO}$ coincide. This observation suggests that the observed EM maximum output power is attributable to a resonance effect between the two layers, which is determined by M_{eff} of LAFO. It should be noted that in Fig. 6, the amplitude of the device's FMR response shows a stepwise increase when $f_{FMR,Py}$ exceeds $f_{FMR,LAFO}$ around $K_{u,LAFO} = -20\,kJ/m^3$. This is likely due to the fact that when $f_{FMR,LAFO} > f_{FMR,Py}$, the Py magnon frequencies fall below the lowest frequency LAFO magnons, impeding the propagation of magnons from the Py layer to the LAFO layer.[30] In contrast, when $f_{FMR,LAFO} < f_{FMR,Py}$, the Py magnons can propagate into the LAFO layer. In addition, since the LAFO layer has an ultralow Gilbert damping, the FMR amplitude is enhanced.

D. Summary

In this work, we investigated the impact of various LAFO parameters on J_{th} and output power of the LAFO/Py/Pt hybrid SHNO using micromagnetic simulations. The results indicate that J_{th} is not significantly affected by changes in t_{LAFO}, $M_{s,LAFO}$, or $K_{u,LAFO}$. However, a peak in the EM output power was observed when $M_{s,LAFO}$ and $K_{u,LAFO}$ are varied. Our findings reveal that the maximum EM output power occurs when $f_{FMR,LAFO}$ and $f_{FMR,Py}$ coincide. Our study also shows that the nature of BM changes between a localized mode and a propagating mode as $K_{u,LAFO}$ varies. Our work provides a roadmap for the engineering of LAFO properties for building more efficient and powerful hybrid SHNO devices for future applications.

ACKNOWLEDGMENTS

The authors acknowledge very helpful discussions with Haowen Ren and Yuri Suzuki. This research was supported by NSF Grant No. DMR-2105114.

AUTHOR DECLARATIONS

Conflict of Interest

The authors have no conflicts to disclose.

Author Contributions

Robert Xi: Data curation (equal); Formal analysis (equal); Investigation (equal); Methodology (equal); Writing – original draft (equal); Writing – review & editing (equal). **Ya-An Lai:** Data curation (equal); Formal analysis (equal); Investigation (equal);

Methodology (equal); Writing – original draft (equal); Writing – review & editing (equal). **Andrew D. Kent:** Conceptualization (equal); Funding acquisition (equal); Supervision (equal); Writing – original draft (equal); Writing – review & editing (equal).

DATA AVAILABILITY

The data that support the findings of this study are available from the corresponding author upon reasonable request.

REFERENCES

[1]A. Khitun, M. Bao, and K. L. Wang, "Magnonic logic circuits," J. Phys. D: Appl. Phys. **43**, 264005 (2010).
[2]J. Han, P. Zhang, J. T. Hou, S. A. Siddiqui, and L. Liu, "Mutual control of coherent spin waves and magnetic domain walls in a magnonic device," Science **366**, 1121 (2019).
[3]V. Demidov, S. Urazhdin, A. Anane, V. Cros, and S. Demokritov, "Spin–orbit-torque magnonics," J. Appl. Phys. **127**, 170901 (2020).
[4]T. Wang and J. Roychowdhury, "OIM: Oscillator-based Ising machines for solving combinatorial optimisation problems," in *International Conference on Unconventional Computation and Natural Computation* (Springer, 2019), pp. 232–256.
[5]T. Makiuchi, T. Hioki, Y. Shimazu, Y. Oikawa, N. Yokoi, S. Daimon, and E. Saitoh, "Parametron on magnetic dot: Stable and stochastic operation," Appl. Phys. Lett. **118**, 022402 (2021).
[6]M. Elyasi, E. Saitoh, and G. E. Bauer, "Stochasticity of the magnon parametron," Phys. Rev. B **105**, 054403 (2022).
[7]R. Sharma, R. Mishra, T. Ngo, Y.-X. Guo, S. Fukami, H. Sato, H. Ohno, and H. Yang, "Electrically connected spin-torque oscillators array for 2.4 GHz WiFi band transmission and energy harvesting," Nat. Commun. **12**, 2924 (2021).
[8]A. Litvinenko, A. Sidi El Valli, V. Iurchuk, S. Louis, V. Tyberkevych, B. Dieny, A. N. Slavin, and U. Ebels, "Ultrafast GHz-range swept-tuned spectrum analyzer with 20 ns temporal resolution based on a spin-torque nano-oscillator with a uniformly magnetized 'free' layer," Nano Lett. **22**, 1874 (2022).
[9]N. Locatelli, V. Cros, and J. Grollier, "Spin-torque building blocks," Nat. Mater. **13**, 11 (2014).
[10]J. Torrejon, M. Riou, F. A. Araujo, S. Tsunegi, G. Khalsa, D. Querlioz, P. Bortolotti, V. Cros, K. Yakushiji, A. Fukushima, H. Kubota, S. Yuasa, M. D. Stiles, and J. Grollier, "Neuromorphic computing with nanoscale spintronic oscillators," Nature **547**, 428 (2017).
[11]S. Tsunegi, T. Taniguchi, K. Nakajima, S. Miwa, K. Yakushiji, A. Fukushima, S. Yuasa, and H. Kubota, "Physical reservoir computing based on spin torque oscillator with forced synchronization," Appl. Phys. Lett. **114**, 164101 (2019).
[12]M. Zahedinejad, A. A. Awad, S. Muralidhar, R. Khymyn, H. Fulara, H. Mazraati, M. Dvornik, and J. Akerman, "Two-dimensional mutually synchronized spin Hall nano-oscillator arrays for neuromorphic computing," Nat. Nanotechnol. **15**, 47 (2019).
[13]M. Romera, P. Talatchian, S. Tsunegi, K. Yakushiji, A. Fukushima, H. Kubota, S. Yuasa, V. Cros, P. Bortolotti, M. Ernoult *et al.*, "Binding events through the mutual synchronization of spintronic nano-neurons," Nat. Commun. **13**, 883 (2022).
[14]D. Marković, M. W. Daniels, P. Sethi, A. D. Kent, M. D. Stiles, and J. Grollier, "Easy-plane spin Hall nano-oscillators as spiking neurons for neuromorphic computing," Phys. Rev. B **105**, 014411 (2022).
[15]H. Kurebayashi, O. Dzyapko, V. Demidov, D. Fang, A. J. Ferguson, and S. Demokritov, "Controlled enhancement of spin-current emission by three-magnon splitting," Nat. Mater. **10**, 660–664 (2011).
[16]M. Balinsky, M. Haidar, M. Ranjbar, P. Dürrenfeld, A. Houshang, A. Slavin, and J. Åkerman, "Modulation of the spectral characteristics of a nano-contact spin-torque oscillator via spin waves in an adjacent yttrium-iron garnet film," IEEE Magn. Lett. **7**, 1 (2016).
[17]C. Safranski, I. Barsukov, H. K. Lee, T. Schneider, A. Jara, A. Smith, H. Chang, K. Lenz, J. Lindner, Y. Tserkovnyak *et al.*, "Spin caloritronic nano-oscillator," Nat. Commun. **8**, 117 (2017).
[18]M. Evelt, C. Safranski, M. Aldosary, V. Demidov, I. Barsukov, A. Nosov, A. Rinkevich, K. Sobotkiewich, X. Li, J. Shi *et al.*, "Spin Hall-induced auto-oscillations in ultrathin YIG grown on Pt," Sci. Rep. **8**, 1269 (2018).
[19]Y. Kajiwara, K. Harii, S. Takahashi, J. Ohe, K. Uchida, M. Mizuguchi, H. Umezawa, H. Kawai, K. Ando, K. Takanashi, S. Maekawa, and E. Saitoh, "Transmission of electrical signals by spin-wave interconversion in a magnetic insulator," Nature **464**, 262 (2010).
[20]X. Y. Zheng, S. Channa, L. J. Riddifor, J. J. Wisser, K. Mahalingam, C. T. Bowers, M. E. McConney, A. T. N'Diaye, A. Vailionis, E. Cogulu, H. Ren, Z. Galazka, A. D. Kent, and Y. Suzuki, "Ultra-thin lithium aluminate spinel ferrite films with perpendicular magnetic anisotropy and low damping," Nat. Commun. **14**, 4918 (2024).
[21]H. Ren, X. Y. Zheng, S. Channa, G. Wu, D. A. O'Mahoney, Y. Suzuki, and A. D. Kent, "Hybrid spin Hall nano-oscillators based on ferromagnetic metal/ferrimagnetic insulator heterostructures," Nat. Commun. **14**, 1406 (2023).
[22]M. Evelt, L. Soumah, A. Rinkevich, S. Demokritov, A. Anane, V. Cros, J. Ben Youssef, G. de Loubens, O. Klein, P. Bortolotti, and V. Demidov, "Emission of coherent propagating magnons by insulator-based spin-orbit-torque oscillators," Phys. Rev. Appl. **10**, 041002 (2018).
[23]L. Chen, K. Zhou, Z. Tao, Z. Gao, L. Liang, Z. Li, and R. Liu, "Self-oscillations in a nanogap spin Hall nano-oscillator with a perpendicularly magnetized external film," Phys. Rev. Appl. **19**, 054051 (2023).
[24]A. Vansteenkiste, J. Leliaert, M. Dvornik, M. Helsen, F. Garcia-Sanchez, and B. Van Waeyenberge, "The design and verification of MuMax3," AIP Adv. **4**, 107133 (2014).
[25]S. I. Kiselev, J. Sankey, I. Krivorotov, N. Emley, R. Schoelkopf, R. Buhrman, and D. Ralph, "Microwave oscillations of a nanomagnet driven by a spin-polarized current," Nature **425**, 380 (2003).
[26]Z. Duan, A. Smith, L. Yang, B. Youngblood, J. Lindner, V. E. Demidov, S. O. Demokritov, and I. N. Krivorotov, "Nanowire spin torque oscillator driven by spin orbit torques," Nat. Commun. **5**, 5616 (2014).
[27]R. D. McMichael and M. D. Stiles, "Magnetic normal modes of nanoelements," J. Appl. Phys. **97**, 10J901 (2005).
[28]M. Succar and M. Haidar, "Spin wave excitations in a nanowire spin Hall oscillator with perpendicular magnetic anisotropy," J. Appl. Phys. **133**, 093901 (2023).
[29]M. Dvornik, A. A. Awad, and J. Åkerman, "Origin of magnetization auto-oscillations in constriction-based spin Hall nano-oscillators," Phys. Rev. Appl. **9**, 014017 (2018).
[30]Y. Fan, J. Finley, J. Han, M. E. Holtz, P. Quarterman, P. Zhang, T. S. Safi, J. T. Hou, A. J. Grutter, and L. Liu, "Resonant spin transmission mediated by magnons in a magnetic insulator multilayer structure," Adv. Mater. **33**, 2008555 (2021).